Available online at www.sciencedirect.com
ScienceDirect
Journal of Power Sources 158 (2006) 1209–1221
JOURNAL OF POWER SOURCES
www.elsevier.com/locate/jpowsour

A new flow field and its two-dimension model for polymer electrolyte membrane fuel cells (PEMFCs)

Xiaochun Zhou, Wenze Ouyang, Changpeng Liu, Tianhong Lu, Wei Xing *, Lijia An

Changchun Institute of Applied Chemistry, Chinese Academy of Sciences, 5625 Renmin Street, Changchun 130022, PR China

Received 13 July 2005; received in revised form 11 October 2005; accepted 13 October 2005
Available online 17 November 2005

Abstract

A new flow field was designed to search flow fields fitting polymer electrolyte membrane fuel cells (PEMFCs) better due its extensible. There are many independent inlets and outlets in the new flow field. The new flow field we named NINO can extend to be more general when pressures at the inlet and outlet vary and some usual flow fields will be obtained. A new mathematical model whose view angle is obverse is used to describe the flow field.

Keywords: Flow field; Mathematical model; PEM fuel cell; Two-dimension; Obverse

1. Introduction

With continuously increasing need of energy and concerning of environment, fuel cell as an effective and clean device to convert energy is attracting more and more researchers. Polymer electrolyte membrane fuel cells (PEMFCs) are considered as highly promising power sources, especially for vehicular applications because of its low-temperature operation and ease of construction. Precise design of flow field and well-chosen operation condition can greatly improve the usage of catalyst, meliorate the wetting state and simplify PEMFC systems [1]. Parallel and interdigitated flow fields [2–4] shown in Fig. 1a and b have their own characteristics. Parallel flow field exhibits lower pressure difference and inhomogeneous reactant gas distribution can easily occur. Products of the electrochemical reactions like water and carbon dioxide can clog single channels, and liquid water can flood the catalyst layer. So liquid water flooding become serious when the flux of gas is small or electrical current is high in parallel flow fields. The forced flow-through-the-electrode characteristic makes the interdigitated flow field offset the disadvantage of the parallel due to that the interdigitated flow field could provide high transport rates of reactant and products to and from the inner catalyst layer. The thickness of diffusion layer in interdigitated flow field is much thinner [3] than that in parallel flow field resulting in that the limiting current and maximum power of PEMFC in interdigitated flow field is higher than that in parallel state. However, the high energy lost in interdigitated flow field is due to the high-pressure drop throughout the PEMFC, and the velocity at the inlet and outlet is extremely high compare to the mid of the flow field because the fluid all crossing the flow field disperses at the inlet and congregates at the outlet.

In order to offset the shortcoming of the two flow fields, a new flow field we named NINO flow field which is the abbreviation of *n*-inlet and *n*-outlet flow field, shown in Fig. 1c, was formed from combination of the two. There are many inlets and outlets in the flow field, the quantity of inlet may be not the same as that of outlet in the new flow field. Every inlet and outlet is independent, and the pressures at these places are varied to extend the new flow field to be more general. The simple situation with symmetric boundary condition of the new flow field was discussed here.

A new mathematical model is presented to describe the new flow field. The models used by other researchers [1–8] were on the whole or part way of channel → gas diffusion layer → cathode → membrane → anode → gas diffusion layer → channel. However, the view here was changed to the obverse of PEMFC, and a two-dimension model was build. This model can be used to optimize the flow field presented above

* Corresponding author. Tel.: +86 431 5262225; fax: +86 431 5685653.
E-mail address: xingwei@ns.ciac.jl.cn (W. Xing).

0378-7753/$ – see front matter © 2005 Elsevier B.V. All rights reserved.
doi:10.1016/j.jpowsour.2005.10.025

Nomenclature

List of symbols

A	area of the flow field (m^2)
b	constant in Eq. (16)
c_{ch}	oxygen concentration in channel ($mol\,m^{-3}$)
c_{GDL}	oxygen concentration in GDL ($mol\,m^{-3}$)
c_o	mol concentration of oxygen gas at the interface of GDL and catalyst layer ($mol\,m^{-3}$)
$c_{o,r}$	reference oxygen concentration ($mol\,m^{-3}$)
c_{o1}	mol concentration of oxygen gas at the interface of GDL and channel ($mol\,m^{-3}$)
c_{o2}	mol concentration of oxygen gas at the interface of channel and bipolar plate ($mol\,m^{-3}$)
c_{oa}	mol concentration of oxygen gas in z-direction ($mol\,m^{-3}$)
c_{wa}	mol concentration of water in z-direction ($mol\,m^{-3}$)
C2, C2′, C2″	symmetry axes
c_o^{in1}	oxygen concentration at inlet1 ($mol\,m^{-3}$)
c_o^{in2}	oxygen concentration at inlet2 ($mol\,m^{-3}$)
c_w^{in1}	water concentration at inlet1 ($mol\,m^{-3}$)
c_w^{in2}	water concentration at inlet2 ($mol\,m^{-3}$)
D_{ch}	diffusion coefficient in channel ($m^2\,s^{-1}$)
D_{GDL}	diffusion coefficient in GDL ($m^2\,s^{-1}$)
D_i	diffusion coefficient in a nonporous system ($m^2\,s^{-1}$)
$D_{i,r}$	reference oxygen diffusion coefficient ($m^2\,s^{-1}$)
D_i^e	effective molecular diffusion coefficient of species i in the gas stream ($m^2\,s^{-1}$)
D_o^e	effective molecular diffusion coefficient of oxygen in the gas stream ($m^2\,s^{-1}$)
D_w^e	effective molecular diffusion coefficient of water in the gas stream ($m^2\,s^{-1}$)
d1	high of the channel (m)
d2	thickness of GDL (m)
E	potential of fuel cell (V)
E_0	open circuit potential (V)
F	Faraday constant (96,487 $C\,mol^{-1}$)
i	species oxygen or water/current density ($A\,m^{-2}$)
$\bar{i}$	average current of the whole fuel cell ($A\,m^{-2}$)
I_o	exchange current density of oxygen ($A\,m^{-2}$)
inlet1	virtual inlet of first kind
inlet2	virtual inlet of second kind
$i(x, y)$	current function($A\,m^{-2}$)
k	transfer coefficient
k_p	permeability of gas diffuser (m^2)
k_{p1}	permeability of gas diffuser in channel (m^2)
k_{p2}	permeability of gas diffuser under shoulder (m^2)
L1	width of ports (m)
L2	width of shoulders (m)
L3	length of the whole flow field (m)
L4	width of the whole flow field (m)
m	pressure changes of one port
M	molecular weight ($kg\,mol^{-1}$)
M_o	molecular weight of oxygen ($kg\,mol^{-1}$)
M_w	molecular weight of water ($kg\,mol^{-1}$)
M_n	molecular weight of nitrogen ($kg\,mol^{-1}$)
n	port number of one side
N	the total the independent condition number
N_{ch}	oxygen flux in channel ($mol\,m^{-2}$)
N_{GDL}	oxygen flux in GDL ($mol\,m^{-2}$)
outlet1	virtual outlet of first kind
outlet2	virtual outlet of second kind
P	total gas pressure (Pa)
P_0	atmospheric pressure (Pa)
r	internal resistance (Ω)
R	gas constant ($J\,mol^{-1}\,K^{-1}$)
s	symmetry center
S_{ch1}	source term in equation of continuity in channel ($mol\,m^{-2}\,s^{-1}$)
S_{sh1}	source term in equation of continuity in GDL ($mol\,m^{-2}\,s^{-1}$)
T	operating temperature (K)
T_r	reference temperature (K)
u_{in1}	velocity at inlet1 ($m\,s^{-1}$)
u_{in2}	velocity at inlet2 ($m\,s^{-1}$)
u_{out2}	velocity at outlet2 ($m\,s^{-1}$)
v	velocity ($m\,s^{-1}$)
x	x-direction
y	y-direction

Greek letters

β	water content
ε	gas diffuser porosity of the GDL
η	overpotential (V)
η_c	cathode overpotential (V)
λ	electro-osmotic drag coefficient of water
μ	air viscosity ($N\,m^{-2}\,s$)
ξ1	dimensionless parameter in Eq. (41)
ξ2	dimensionless parameter in Eq. (41)
ρ	density of the fluid ($kg\,m^{-3}$)
σ	internal conductivity of the fuel cell ($S\,m^2$)
σ1, σ2, σ3	symmetry planes

Superscripts and subscripts

H^+	proton
i	species
e	effective
n	nitrogen
o	oxygen
w	water
r	reference
in1	inlet1
in2	inlet2
out1	outlet1
out2	outlet2

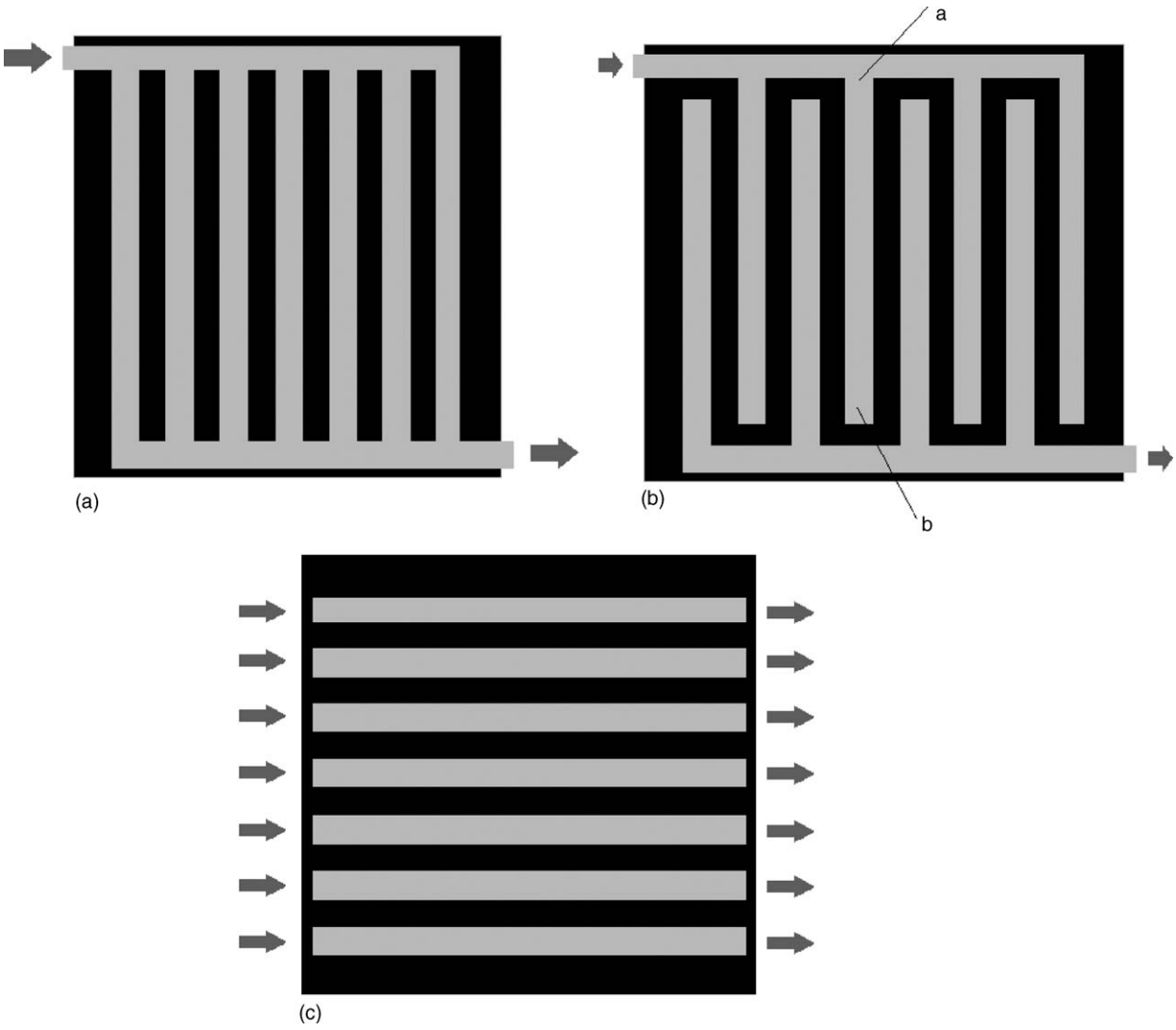

Fig. 1. Air flow fields for PEMFC (a) parallel, (b) interdigitated and (c) NINO.

and help us to understand the whole situation of all kinds of flow fields. It is helpful to the job of thinning [9] PEMFC because the difference of species is small in z-direction in thin flow field. The cathode side of the new flow field was studied, and some effect of base parameter was considered.

2. New flow field and mathematical model

2.1. New flow field

The new flow field shown in Fig. 2 has five inlets and outlets, respectively. The quantity of the inlet and outlet can vary as you need. Each inlet and outlet is independent and can connect to the pipeline. The inlets and outlets can exchange with or transform to each other, then the general flow field will be got.

If the flow field has $2n$ ports and each port has m pressure changes, the glancing number of the pressure change can be given as follows,

$$N = m^{2n} \tag{1}$$

where N is the total independent condition number, if the pressures at every port are the same, the fluid neither can come into the flow field nor can go out. In this situation, the flow field cannot work in the course of nature, and the number must be subtracted.

$$N = m^{2n} - m \tag{2}$$

Considering the symmetry of the flow field, the number will be smaller than the one given above. In the flow field, there are three symmetry planes ($\sigma 1$, $\sigma 2$, $\sigma 3$), three symmetry axes (C2, C2′, C2″) and one symmetry center(s) shown in Fig. 2. If every port is in the same position after operations of two symmetry elements, the two symmetry elements have the same effect on the flow field. For example, the anticlockwise order of the port is 1, 2, 3, 4, 5, 10, 9, 8, 7, 6 before operation, and became 5, 4, 3, 2, 1, 6, 7, 8, 9, 10 after operation of $\sigma 1$ or C2. So the $\sigma 1$ and C2 have the same effects on the NINO, and we only need to consider one of them. The operation of $\sigma 2$ and C2′, C2″ and s have the same condition. After the operation of $\sigma 3$, every port is in the former position and the result will not be effected by this

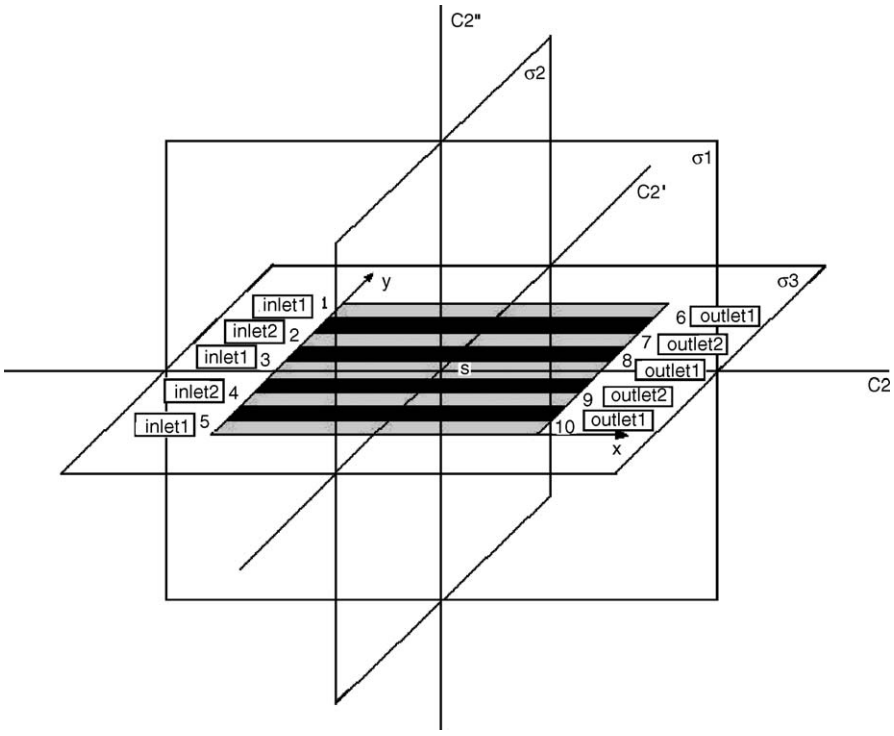

Fig. 2. The extension of the novel flow field.

operation. As a result, we only need to consider the operation of σ1, σ2 and *s*.

When the ports are set to some pressures, after the operation of C2, the condition become superposable with that before the operation, then this condition only appears one time under this operation. If the condition is not superposable with the former, this condition appears twice under this operation. The things above will happen in both σ2, C2′ and C2″, *s*. These conditions appearing repeatedly must be subtracted from the quantity calculated from Eq. (2). But if the results are the same after the operation of C2 and C2′, or C2 and C2″, or C2′ and C2″, it is needed to add the number calculated here. Then the independent condition can be described as follows,

$$N = m^{2n} - m - \mathrm{N1} - \mathrm{N2} - \mathrm{N3} + \mathrm{N4} + \mathrm{N5} + \mathrm{N6} \quad (3)$$

where N1 is the unsuperposition number after operation of C2 or σ1, N2 is the unsuperposition number after operation of C2′ or σ2, N3 is the unsuperposition number after operation of C2″ or σ3, N4 is the superposition number after operation of C2 and C2′, N5 is the superposition number after operation of C2 and C2″, N6 is the superposition number after operation of C2′ and C2″.

If the pressures at the ports are changed, some interesting results will be got. First, if the port 6 and port 7, 2 and 3, 8 and 9, 4 and 5 are combined, respectively, the NINO flow field will become the serpentine flow field [5]. Second if the ports 1, 2, 3, 4, 5 are combined directly, and ports 6, 7, 8, 9, 10 are combined too, but the pressure of the two kinds of ports is different, the NINO flow field will be the parallel one. Third if the ports 1, 3, 5 have the same pressure, and 7, 9 have the same pressure, but the pressure is different of the two kinds of ports, the NINO flow field will be the interdigitated one. From the analysis above, it is found that the parallel, interdigitated and serpentine flow field can all be gained from the NINO flow field at some extreme operation condition. Except for the three flow fields, there are almost infinity flow field which can are got from the new flow fields, if the operation condition was changed. Thereby which is the best one becomes the question that attracts us very much. To answer this question, a new mathematic model is presented as follows.

2.2. Model development

The PEMFC model described here is developed to study the effect of the porous layer in the flow field and the velocity variation at the port. Consequently, to avoid complexities, we decided to develop the half-cell model for the cathode side of the fuel cell. It was assumed that gas in the flow field was air on the cathode side. The air enters the domain at gas inlet in the bipolar plate. The flow field in the bipolar plate helps in the distribution of reactant gas onto the surface of the electrode.

2.2.1. Problem domain

The base dimensions for channel width, shoulder width and the whole flow field are shown in Fig. 3. Since it is very complex to optimize the novel flow field, some base cases are discussed. The main content will be concentrate on the method of finding the answer. The velocity at ports 1, 3, 5, ports 2, 4, ports 6, 8, 10, was set at u_{in1}, u_{in2}, u_{out2}, respectively, and the pressure at ports 7, 9 is 1.00 atm. The proportion of the permeability in the channel to the permeability under the shoulder will varied from 20:1 to 100:1. The permeability of gas diffuser under shoulder and in

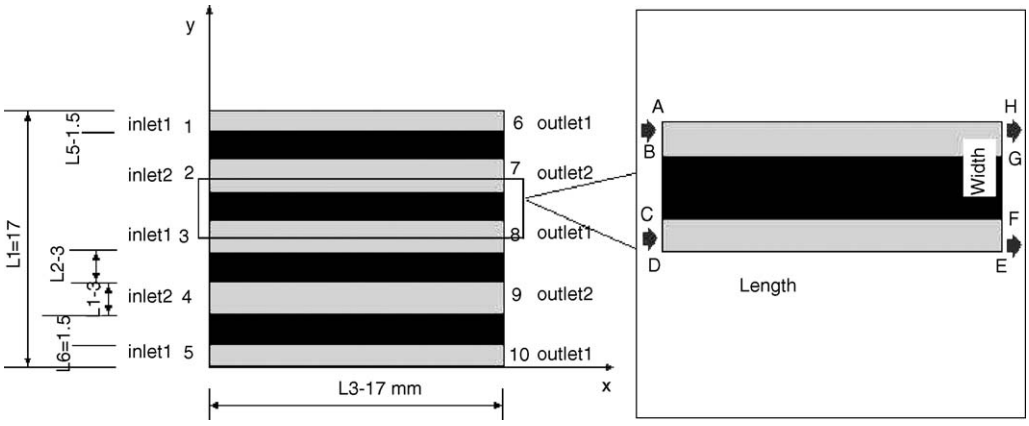

Fig. 3. The base dimensions for channel width, shoulder width and the whole flow field.

channel varies from $0.5 \times 1.76 \times 10^{-11}$ to $1.3 \times 1.76 \times 10^{-11}$, but the proportion will not change. The effect of width of shoulder and channel is studied also.

2.2.2. Model assumptions

The numerical model assumes that

1. The PEM fuel cell operates under steady state condition [4].
2. There are no temperature changes in the PEM fuel cell, i.e. isothermal operation [4].
3. Laminar flow exists everywhere in the gas channels and all the transport equations were formulated for laminar behavior [7].
4. Porous media exists in the gas diffusers is isotropic.
5. Gas in flow field is ideal gas and uncompress, because the pressure drop throughout the flow field is very small.
6. Water produced from reaction only exist in gas, in this paper we do not consider the liquid water in channel [4].

Actually, assumptions 1–4 are usually considered as standard assumptions in many papers [10–15].

2.2.3. Governing transport equations

The reaction equation of cathode is

$$O_2 + 4H^+ + 4e^- \rightarrow 2H_2O \tag{4}$$

The conservation of mass, also called equation of continuity in channel is given by [4]:

$$-\frac{\partial(\rho v_x)}{\partial x} - \frac{\partial(\rho v_y)}{\partial y} = S_{\text{ch1}} \tag{5}$$

where ρ is the density of the fluid in the medium, v_x and v_y are velocities in the x- and y-direction and S_{ch1} is the source term. This source term includes the H^+ and water transferring from anode,

$$S_{\text{ch1}} = \frac{M_{H^+} i}{F} + \frac{M_w \lambda i}{F} \tag{6}$$

F is the faraday constant, λ the electro-osmotic drag coefficient of water, and i is the current density. Darcy's law neglecting the effect of gravity for fluid flow through a porous medium is,

$$v_x = -\frac{k_{\text{p1}}}{\mu}\frac{\partial P}{\partial x} \tag{7}$$

$$v_y = -\frac{k_{\text{p1}}}{\mu}\frac{\partial P}{\partial y} \tag{8}$$

where k_{p1} is the permeability in channel, μ the viscosity of the fluid in the medium, and P is the total gas pressure. Here we assume that the channel is filled with porous material with high permeability. In fact, the difference of permeability in channel and under shoulder represents the distribution ability of flow medium in them. Darcy's law is related to the Hagen–Poiseuille equation for laminar flow in the gas channel. The k_{p1} an μ are assumed to be constant.

When Eqs. (7) and (8) are substituted into Eq. (5), we obtain,

$$-\frac{\partial(-(\rho k_{\text{p1}}/\mu)(\partial P/\partial x))}{\partial x} - \frac{\partial(-(\rho k_{\text{p1}}/\mu)(\partial P/\partial y))}{\partial y} = S_{\text{ch1}} \tag{9}$$

There are three species that are oxygen, water and nitrogen in an air cathode. Oxygen is fed to the electrode interface, water is generated at the gas diffusion layer (GDL)/electrode interface. When oxygen reacts at the GDL/electrode interface, the Tafel type equation is obtained to describe the current distribution along the catalyst layer.

$$i = I_o \frac{c_o}{c_{o,r}} \exp\left(\frac{4kF}{RT}\eta\right) \tag{10}$$

where I_o is the exchange current density of oxygen, c_o the mole concentration of oxygen gas in catalyst layer, $c_{o,r}$ the reference oxygen concentration, and k is the transfer coefficient.

If the average oxygen concentration in channel and its diffusion layer is c_{oa}, and the distribution is linear shown in Fig. 4, the relationship of c_{oa}, c_o, c_{o1}, c_{o2} is

$$c_{oa} = \frac{((c_o + c_{o1})\text{d2})/2 + ((c_{o1} + c_{o2})\text{d1})/2}{\text{d1} + \text{d2}} \tag{11}$$

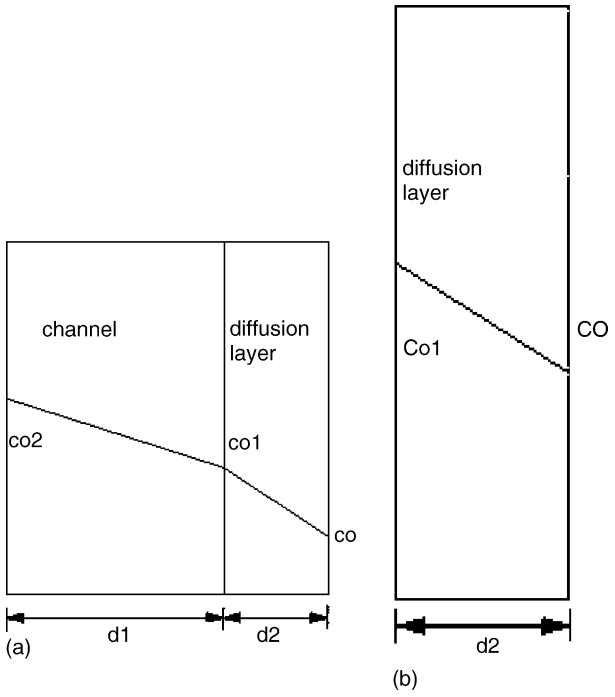

Fig. 4. Oxygen concentration (a) in channel and its diffusion layer, and (b) in diffusion layer under shoulder.

where d1 is the height of channel, and d2 is the thickness of GDL. According Fick's law, oxygen flux in channel can be determined

$$N_{\mathrm{ch}} = D_{\mathrm{ch}} \frac{\partial c_{\mathrm{ch}}}{\partial x} \tag{12}$$

Oxygen flux in GDL is

$$N_{\mathrm{GDL}} = D_{\mathrm{GDL}} \frac{\partial c_{\mathrm{GDL}}}{\partial x} \tag{13}$$

If there is no chemical reaction in the flow field, the mass balance used for oxygen and water vapor can be described as follows,

$$D_i^{\mathrm{e}} \frac{\partial^2 c_i}{\partial x^2} + D_i^{\mathrm{e}} \frac{\partial^2 c_i}{\partial y^2} - v_x \frac{\partial c_i}{\partial x} - v_y \frac{\partial c_i}{\partial y} = 0 \tag{14}$$

where i represent oxygen or water, D_i^{e} is the effective molecular diffusion coefficient of species i in the gas stream, and c_i is the average mol concentration of species i in channel. The relationship of D_i^{e} and D_i which is the diffusion coefficient in a nonporous system is given:

$$D_i^{\mathrm{e}} = D_i \varepsilon^{1.5} \tag{15}$$

where ε is the porosity of the channel. In this model, the porosities and the effective diffusion coefficients of the gases are assumed to be constant and invariant of pressure. The relation between temperature and the diffusion coefficient is given,

$$D_i = D_{i,\mathrm{r}} \left(\frac{T}{T_{\mathrm{r}}} \right)^b \tag{16}$$

where $D_{i,\mathrm{r}}$ is the reference oxygen or water diffusion coefficient, T the operation temperature, and T_{r} is the reference temperature.

From Fig. 3, when the chemical reaction takes place at any point of the flow field plane, the oxygen balance is got from Eq. (14):

$$D_{\mathrm{o}}^{\mathrm{e}} \frac{\partial^2 c_{\mathrm{oa}}}{\partial x^2} + D_{\mathrm{o}}^{\mathrm{e}} \frac{\partial^2 c_{\mathrm{oa}}}{\partial y^2} - v_x \frac{\partial c_{\mathrm{oa}}}{\partial x} - v_y \frac{\partial c_{\mathrm{oa}}}{\partial y} + \frac{i}{4F} = 0 \tag{17}$$

where $i/4F$ represent the consumption of oxygen, c_{oa} represents mole concentration of oxygen. The equations of water vapor balance is got from Eq. (14) also:

$$D_{\mathrm{w}}^{\mathrm{e}} \frac{\partial^2 c_{\mathrm{wa}}}{\partial x^2} + D_{\mathrm{w}}^{\mathrm{e}} \frac{\partial^2 c_{\mathrm{wa}}}{\partial y^2} - v_x \frac{\partial c_{\mathrm{wa}}}{\partial x} - v_y \frac{\partial c_{\mathrm{wa}}}{\partial y} - \frac{(1+2\lambda)i}{2F} = 0 \tag{18}$$

where $(1+2\lambda)i/2F$ represents the production of water vapor, and c_{wa} represents mole concentration of water.

Under shoulder the conservation of mass equation is

$$-\frac{\partial(\rho v_x)}{\partial x} - \frac{\partial(\rho v_y)}{\partial y} = S_{\mathrm{sh1}} \tag{19}$$

$$S_{\mathrm{ch1}} = \frac{M_{\mathrm{H^+}} i}{F} + \frac{M_{\mathrm{w}} \lambda i}{F} \tag{20}$$

Darcy's law neglecting the effect of gravity for fluid flow through a porous medium is,

$$v_x = -\frac{k_{\mathrm{p2}}}{\mu} \frac{\partial P}{\partial x} \tag{21}$$

$$v_y = -\frac{k_{\mathrm{p2}}}{\mu} \frac{\partial P}{\partial y} \tag{22}$$

The k_{p2} and μ are assumed to be constant. When Eqs. (21) and (22) are substituted into Eq. (19), we obtain,

$$-\frac{\partial(-(\rho k_{\mathrm{p2}}/\mu)(\partial P/\partial x))}{\partial x} - \frac{\partial(-(\rho k_{\mathrm{p2}}/\mu)(\partial P/\partial y))}{\partial y} = S_{\mathrm{sh1}} \tag{23}$$

The Tafel type equation is obtained to describe the current distribution along the catalyst layer.

$$i = I_{\mathrm{o}} \frac{c_{\mathrm{o}}}{c_{\mathrm{o,r}}} \exp\left(\frac{4kF}{RT} \eta \right) \tag{24}$$

If the average oxygen concentration in diffusion layer is c_{a}, and the distribution is linear, the relationship of c_{oa}, c_{o} and c_{o1} shown in Fig. 4b is

$$c_{\mathrm{oa}} = \frac{c_{\mathrm{o}} + c_{\mathrm{o1}}}{2} \tag{25}$$

According Fick's law, oxygen flux in GDL can be determined

$$N_{\mathrm{GDL}} = D_{\mathrm{GDL}} \frac{\partial c_{\mathrm{GDL}}}{\partial x} \tag{26}$$

The equations of oxygen and water balance in GDL are the same as the ones in channel.

2.2.4. Boundary conditions

There are four shoulders that can be changed as we need in this flow field. Ports 1, 3, 5 having the same flux velocity belong to the inlet1; ports 2, 4 belong to the inlet2 which have two

times flux velocity to inlet1; ports 6, 8, 10 having the same flux velocity to inlet2 belong to the outlet1; ports 7, 9 belong to the outlet2 whose pressure was set to 1 atm. All ports have the same width L1 and all shoulders' width is L2. The whole length and width of flow field is L3 and L4.

In order to make the result figures more clear and reduce calculation, symmetry boundary condition was applied in this paper, and part of the flow field shown in Fig. 3 was simulated. In Fig. 3,

$$\mathrm{AB} = \mathrm{CD} = \mathrm{L1}/2 \tag{27}$$

$$\mathrm{EF} = \mathrm{GH} = \mathrm{L1}/2 \tag{28}$$

$$\mathrm{BC} = \mathrm{GF} = \mathrm{L2} \tag{29}$$

$$\mathrm{DE} = \mathrm{AH} = \mathrm{L3} \tag{30}$$

At the inlet2 AB, where the reactant gases are fed to the electrode, the pressure and the mole concentration of each species are specified as follows,

$$c_\mathrm{o} = c_\mathrm{o}^{\mathrm{in2}}, \qquad c_\mathrm{w} = c_\mathrm{w}^{\mathrm{in2}}, \qquad \frac{\partial P}{\partial x} = -\frac{\mu}{k_{\mathrm{p1}}} u_{\mathrm{in2}} \tag{31}$$

At the inlet1 CD, the mole concentration of each species are specified as follows,

$$c_\mathrm{o} = c_\mathrm{o}^{\mathrm{in1}}, \qquad c_\mathrm{w} = c_\mathrm{w}^{\mathrm{in1}}, \qquad \frac{\partial P}{\partial x} = -\frac{\mu}{k_{\mathrm{p1}}} u_{\mathrm{in1}} \tag{32}$$

At the outlet1 EF, where the reactant gases flow out of the electrode, the pressure and the mole concentration of each species are specified as follows,

$$\frac{\partial c_\mathrm{o}}{\partial x} = 0, \qquad \frac{\partial c_\mathrm{w}}{\partial x} = 0, \qquad P = P_0 \tag{33}$$

At the outlet2 GH, the mole concentration of each species are specified as follows,

$$\frac{\partial c_\mathrm{o}}{\partial x} = 0, \qquad \frac{\partial c_\mathrm{w}}{\partial x} = 0, \qquad \frac{\partial P}{\partial x} = -\frac{\mu}{k_{\mathrm{p1}}} u_{\mathrm{out2}} \tag{34}$$

At the boundaries AH, DE, Newman boundaries condition was used

$$\frac{\partial c_\mathrm{o}}{\partial y} = 0, \qquad \frac{\partial c_\mathrm{w}}{\partial y} = 0, \qquad \frac{\partial P}{\partial y} = 0 \tag{35}$$

At the boundaries BC, FG

$$\frac{\partial c_\mathrm{o}}{\partial x} = 0, \qquad \frac{\partial c_\mathrm{w}}{\partial x} = 0, \qquad \frac{\partial P}{\partial x} = 0 \tag{36}$$

3. Numerical techniques and procedures

The model equations developed above are coupled closely, so the whole set of equations must be solved simultaneously and iteratively. First we solved the pressure Eqs. (9) and (23) with the concentration of water and oxygen was set. The gas density can be calculated by

$$\rho = (M_\mathrm{o} - M_\mathrm{w})c_\mathrm{oa} + (M_\mathrm{n} - M_\mathrm{w})c_\mathrm{na} + PM_\mathrm{w}/RT \tag{37}$$

where M_o, M_w and M_n represent molecular weight of oxygen, water and nitrogen, respectively. c_na is the average nitrogen concentration. Then the velocity in flow field will be got from Darcy's law.

Next Eq. (17) of oxygen concentration will be solved. But the current density i is a function of oxygen concentration, and the function in channel is different from the one under shoulder.

In channel, the oxygen flux in channel and in GDL are equal to each other, and the relationship of oxygen concentration in channel and in GDL can be got from Eqs. (12) and (13),

$$N_\mathrm{ch} = D_\mathrm{ch}\frac{\partial c_\mathrm{ch}}{\partial x} = N_\mathrm{GDL} = D_\mathrm{sh}\frac{\partial c_\mathrm{GDL}}{\partial x} \tag{38}$$

Assuming the concentration variation is linear, Eq. (38) can be reduced

$$D_\mathrm{ch}\frac{c_{\mathrm{o}2} - c_{\mathrm{o}1}}{\mathrm{d1}} = D_\mathrm{GDL}\frac{c_{\mathrm{o}1} - c_\mathrm{o}}{\mathrm{d2}} \tag{39}$$

In addition,

$$N_\mathrm{GDL} = \frac{i}{4F} = I_\mathrm{o}\frac{c_\mathrm{o}}{4Fc_{\mathrm{o,r}}}\exp\left(\frac{4kF}{RT}\eta\right) \tag{40}$$

Combining Eqs. (11), (39) and (40)

$$c_\mathrm{o} = \frac{2}{4 + \xi 1 + 3\xi 2}c_\mathrm{oa} \tag{41}$$

where dimensionless parameter

$$\xi 1 = I_\mathrm{o}\frac{c_\mathrm{o}\mathrm{d1}}{4FD_\mathrm{ch}c_{\mathrm{o,r}}}\exp\left(\frac{4kF}{RT}\eta\right) \tag{42}$$

$$\xi 2 = I_\mathrm{o}\frac{c_\mathrm{o}\mathrm{d2}}{4FD_\mathrm{GDL}c_{\mathrm{o,r}}}\exp\left(\frac{4kF}{RT}\eta\right) \tag{43}$$

Under shoulder, there is only GDL. Combining Eqs. (25), (26) and (40), the concentration c_oa, c_o

$$c_\mathrm{o} = \frac{2}{2 + \xi 2}c_\mathrm{oa} \tag{44}$$

After solving Eq. (17), the result of oxygen concentration was applied to solve Eq. (18) to get the distribution of water concentration.

The equations were solved iteratively with finite-difference method, and the solution was considered to be convergent when the relative error between two consecutive iterations was less than 10^{-5}. Stringent numerical tests were performed to ensure that the solutions were independent of the grid size. An 80×60 (length $\times$ width) mesh was found to provide sufficient spatial resolution.

4. Results and discussion

In parallel flow field, the fluid mainly flows in channels, and the velocity under shoulders is nearly zero. Diffusion is the main way for the components to transport between the place in channel and under shoulder. So reducing the width of shoulder is advantageous to components' transportation, but narrow shoulders will increase difficulty of manufacture.

In interdigitated flow field, the fluid flows not only in channels but also under shoulders. The pressure difference between two neighbor channels forces the fluid to flow under shoulder, and the components' transportation under shoulder in interdigitated flow field becomes much better than that in parallel flow field. As a result, the interdigitated flow field performs better at high mass-transport limiting current density as compared to the parallel flow field [3]. But the velocity at the end part of channels (around b position shown in Fig. 1b) is much slower than that at the start part of channels (around a position shown in Fig. 1b), and the reactant concentration at this part will be relative low. What's more, high velocity in GDL and catalyst layer cause the catalyst layer and membrane dehydrate, and increase ohmic overpotential, when no water is added to humidify the cathode inlet air. So the interdigitated flow field performs worse at low or middle current density as compared to the parallel flow field [2]. In addition, in order to keep a certain fluid flux, higher pressure must be applied to the interdigitated flow field with the increasing of lost power consumed by fuel cell system itself.

Combining the two flow fields, a new flow field is shown in Fig. 1c forms. Because of velocity difference of the neighbor inlets and outlets, the pressure difference between the neighbor channels is generated to force part of fluid to flow through the GDL under shoulder. So the two neighbor channels will served as interdigitated flow field, and the shear force of gas stream helps removing the liquid water result in reducing the electrode-flooding problem, and the oxygen concentration will increase. On the other hand, the velocity in channels is relative high because of higher velocity at each outlet (end part of channels).

Because each port in NINO is independent, every port can be fixed to be inlet or outlet. From studying of NINO, almost infinity flow field modes will be obtained, and through the studying of these modes, it is forecast that some outstanding flow field will be found to be suit to PEMFC. The flow field with two kinds of inlets (inlet1 and inlet2) and two kinds of outlets (outlet1 and outlet2) was studied here. The parameters were shown in Table 1. Inlet1 to outlet1 and inlet2 to outlet2 served as a parallel and have high velocity. As a result, the oxygen in channel renews very fast and current under channel will increase. Especially, when the feed is not gas but methanol, a mount of CO_2 gas will be generated at high current density, and the channel will be filled with CO_2 gas [16]. At this time, removing CO_2 gas instead of increasing inlet velocity becomes important. Inlet1 to outlet1 and inlet2 to outlet2 can achieve this goal, because relative high velocity in channel from inlet to outlet.

In order to describe the flow field and optimize the NINO flow field, a new simple model is given. Considering the complex of optimization, some simple conditions were studied and optimizing work will be reported later.

4.1. Model validation

To validate the current two-dimension model, comparisons are made to the experimental data of Ticianelli et al. [17] for a single cell. The schematic of the computation domains is presented in Fig. 3, and the basic parameters used in the model validation are given in Table 1.

The mathematic model developed above can produce cathode (or anode by modification) polarization data of voltage versus

Table 1
Conditions and parameters

Parameter	Value	Source
Number of the shoulders	4	
Width of the channel beside port1 and port5, L1 (m)	3×10^{-3}	
Width of the shoulder, L2 (m)	3×10^{-3}	
Length of the whole flow field, L3 (m)	27×10^{-3}	
Width of the whole flow field, L4 (m)	27×10^{-3}	
Width of the port1, L5 (m)	1.5×10^{-3}	
Width of the port5, L6 (m)	1.5×10^{-3}	
High of channel, d1 (m)	1×10^{-3}	
Thickness of GDL, d2 (m)	3×10^{-4}	
Air viscosity, μ (N m^{-2} s)	$1.38 \times 10^{-5}(T/298)^{1.02}$	[22]
Permeability of gas diffuser under shoulder, kp2 (m^2)	1.76×10^{-11}	[4]
Permeability of gas diffuser in channel, kp1 (m^2)	1.76×10^{-9}	Assuming
Gas diffuser porosity, ε	0.4	[23]
Oxygen diffusivity in gas, D_o (m^2 s^{-1})	$1.775 \times 10^{-5}(T/273.15)^{1.5}$	[4]
Water diffusivity in gas, D_w (m^2 s^{-1})	$2.56 \times 10^{-5}(T/307.15)^{1.5}$	[4]
Transfer coefficient of oxygen reduction reaction, k	0.5	[4]
Reference oxygen concentration, $c_{o,r}$ (mol m^{-3})	34.5	Calculated value
Exchange current density of oxygen concentration reaction, I_o (A m^{-2})	100	[24]
Faraday constant, F (C mol^{-1})	97487	
Operating temperature, T (K)	353.15	
b	1.5	[7]
Cathode overpotential, η (V)	0.1	
Atmospheric pressure, P_0 (Pa)	101325	
Cathode oxidant stoichiometric flow ratio	1.68	Assuming
Pressure at outlet1 (Pa)	P_0	
Electro-osmotic drag coefficient of water	1	[3]

current density. To validate the model with data of single fuel cell, the other parts of fuel cell were assumed to be a resistance because of the high activity of transport and reaction for hydrogen such as high diffusion coefficient and high exchange current [3]. The internal conductivity of the fuel cell was set to be 4×10^4 S m^2 at 353 K from the experiment data fitting, and it varied with temperature by [18]:

$$\sigma = \exp\left[1268\left(\frac{1}{303} - \frac{1}{T}\right)\right](5139\beta - 3260) \quad (45)$$

where β is the water content, and it is set to be constant. Combining the conductivity got from fitting result and Eq. (45), the conductivity at different temperature is

$$\sigma = 4 \times 10^4 \exp\left[1268\left(\frac{1}{353.15} - \frac{1}{T}\right)\right] \quad (46)$$

The exchange current density of oxygen reaction is given by [19]:

$$I_o = 10^{3.507-4001/T} \quad (47)$$

The relationship of voltage and current density is

$$E = E_0 - \eta_c - \bar{i}r \quad (48)$$

where E is the voltage of cell, E_0 the thermodynamic open circuit potential, $\bar{i}$ the average current density, and r the internal resistance of cell.

The curves in Fig. 5 are the numerically prediction showing good agreement with the newly selected experimental voltage versus current density at the different operating temperature, then the model is proved to be an accurate model.

4.2. Base case

Fig. 6 shows the pressure distribution all through the flow field. The pressure difference is smooth in channel and sharp under shoulder. It is mainly because the permeability (kp1) in channel is 100 times bigger than under shoulders (kp2) and pressure difference between two channels is obvious.

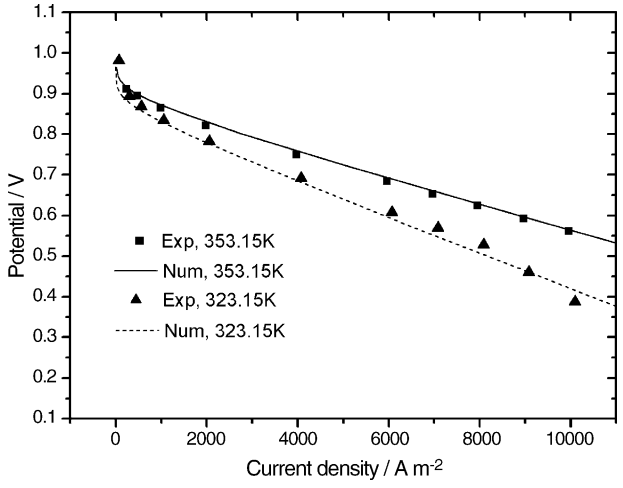

Fig. 5. Comparison of numerically predicted polarization curves with experimental data.

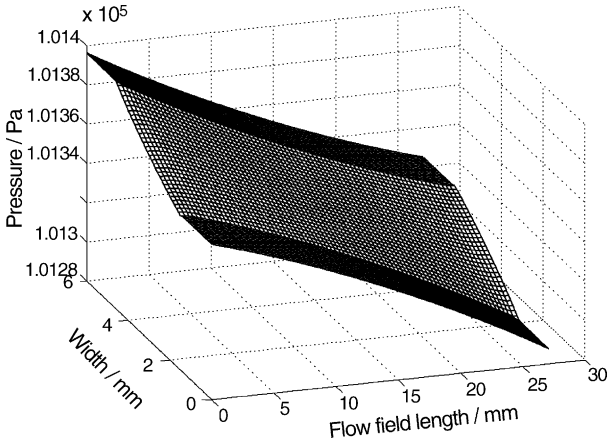

Fig. 6. Pressure distribution in the NINO for the base case.

The profiles of x-directions, y-directions and average velocity are given in Figs. 7–9. The x-direction velocity in channel decreases along x-direction in high-pressure channel and it is much higher than that under shoulders. The highest y-direction velocity appears in channel near the ports, because the flow rate near the ports is much bigger than that at other parts of the flow field. Here the pressure difference in y-direction under shoulders is sharp. As a result, the velocity under shoulder is mainly along y-direction. When the velocity of the ports varies, the inlets

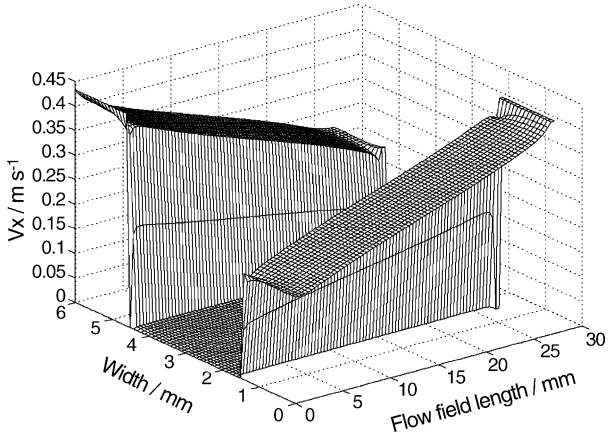

Fig. 7. x-Direction velocity distribution in the NINO for the base case.

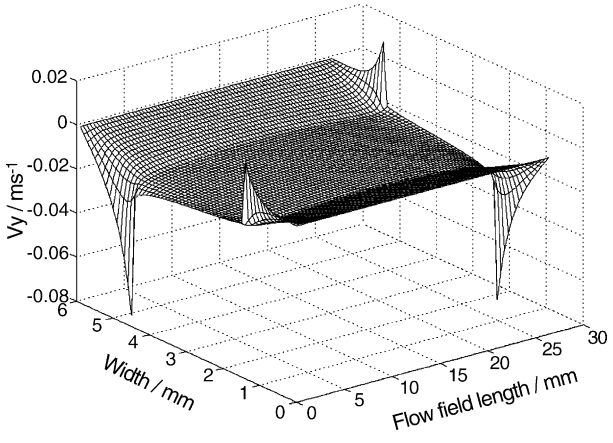

Fig. 8. y-Direction velocity distribution in the NINO for the base case.

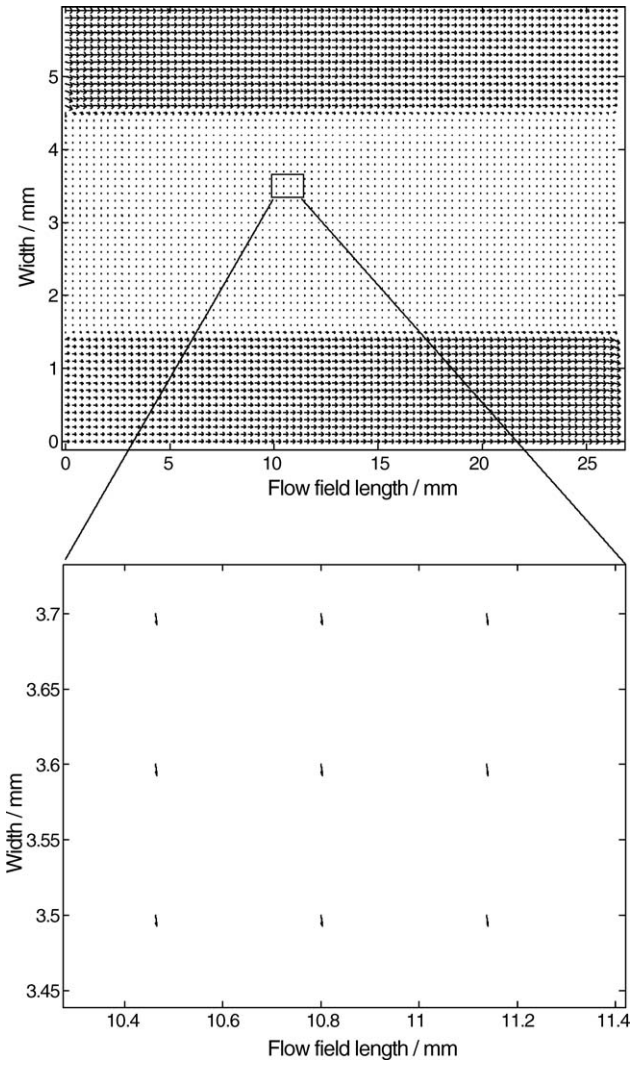

Fig. 9. Average velocity distribution in the NINO for the base case.

and outlets will transform and the velocity under shoulder will change. Using this method all kinds of different flow fields can be studied, and some good ones will be selected.

The oxygen distribution is shown in Fig. 10. The concentration of oxygen decreases along the channel and reach the lowest near the outlet2. Since the velocity in channel is very high, the concentration decreases slowly. But the concentration changes very fast under shoulders, because of the consumption and slow velocity. In addition, we know from Eq. (10) that the current distribution corresponds to the oxygen distribution shown in Fig. 10. The shape of this figure is similar to the result of conventional flow field [20]. But the vale of oxygen concentration under shoulder is not symmetric because of y-direction velocity.

The water vapor distribution shown in Fig. 11 has the opposite trends. The water vapor generated in flow field comes from two ways: first, the water was generated at the place where the oxygen was consumed; second, net water transports with proton transportation from anode to cathode. The velocity under shoulders is slower than in channels, and the water concentration under shoulders becomes higher than in channel. The highest concentration of water appears near the outlet2. When the electrode overpotential is changed, and the corresponding current densities are obtained from the following equation:

$$\bar{i} = \frac{1}{A}\int i(x, y)\,\mathrm{d}s \tag{49}$$

where $\bar{i}$ represents the average current of the whole fuel cell, A represents the area of the electrode, and $i(x, y)$ is the current function. The polarization curve for the base case shown in Fig. 5 is also obtained. The average current density for the base case is 0.9226 A cm^{-2}.

4.3. Effect of permeability of gas diffuser (kp2) under shoulder

Fig. 12 shows the effect of kp2 variation on the pressure distribution at $x = 0.5$L3. The values of kp2 include $0.5 \times 1.76 \times 10^{-11}$, $0.7 \times 1.76 \times 10^{-11}$, $0.9 \times 1.76 \times 10^{-11}$, $1.1 \times 1.76 \times 10^{-11}$ and $1.3 \times 1.76 \times 10^{-11}$ with the other parameters keeping as base case. The proportion of kp1:kp2 will not be changed. The distributions of velocity, oxygen concentration and water concentration have the same value calculated from the model, but the pressure decreases dramatically in high-pressure channel shown in Fig. 12 when kp2 increased. This is

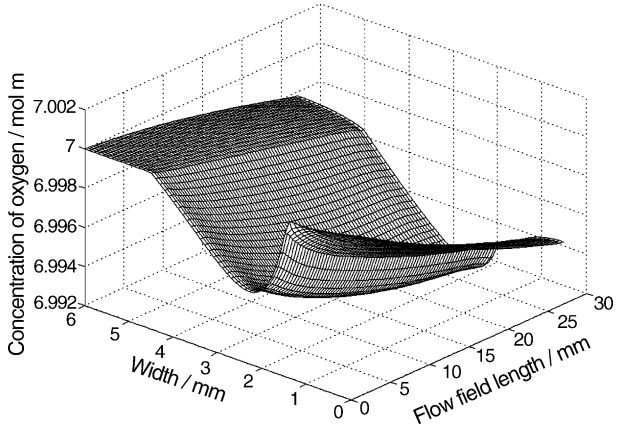

Fig. 10. Oxygen distribution in the NINO for the base case.

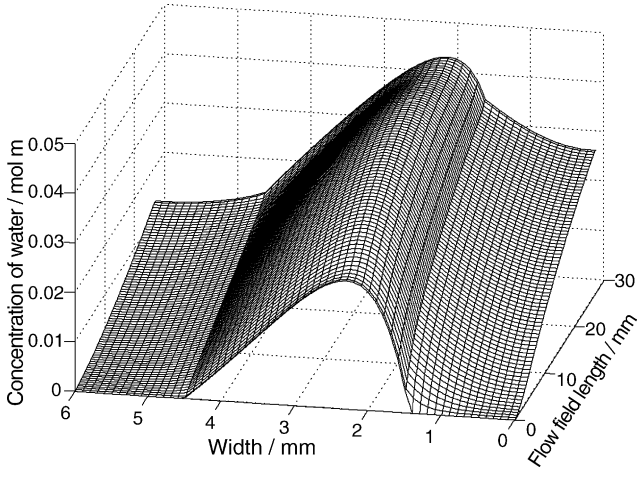

Fig. 11. Water vapor distribution in the NINO for the base case.

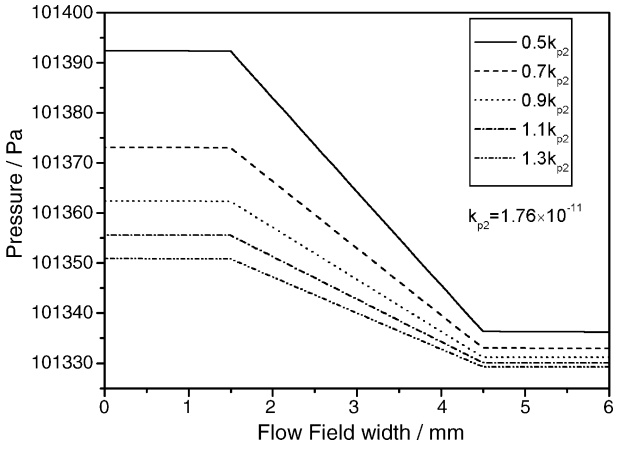

Fig. 12. Effect of permeability of gas diffuser under shoulder on pressure distribution at $x = 0.5L3$.

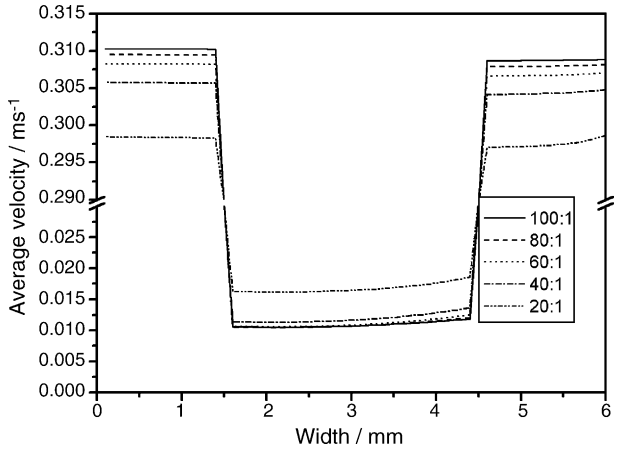

Fig. 14. Effect of the proportion of kp1 to kp2 on average velocity distribution at $x = 0.5L3$.

mainly because of applying of the velocity boundary conditions. The dramatic variation of pressure can be easily explained by Eqs. (7) and (8).

4.4. Effect of the proportion of kp1 in channels to kp2 under shoulders (kp1:kp2)

The effect of kp1:kp2 (kp1 represent the kp in channels, kp2 represent the kp under the shoulders) is investigated. When kp1:kp2 is in case of 20:1, 40:1, 60:1, 80:1, 100:1, the effect of these variations was studied with the other parameters being same as base case. The effects of vary aspects are shown from Figs. 13–16. When we changed the proportion, the kp2 was kept in 1.76×10^{-11} m^2. Fig. 13 shows that, as the increasing of the proportion, the pressure increases both in high-pressure channel and in low-pressure channel. Especially at the proportion of 20:1, the pressure difference trends to be small. That is to say, increasing the proportion can undulate the pressure distribution in the NINO flow field. But this trend becomes weak when the proportion of kp1 to kp2 increases up to 60:1. The effect on the velocity was shown in Fig. 14, the velocity increases with the rising of kp1 in channel while decreases under shoulder, and

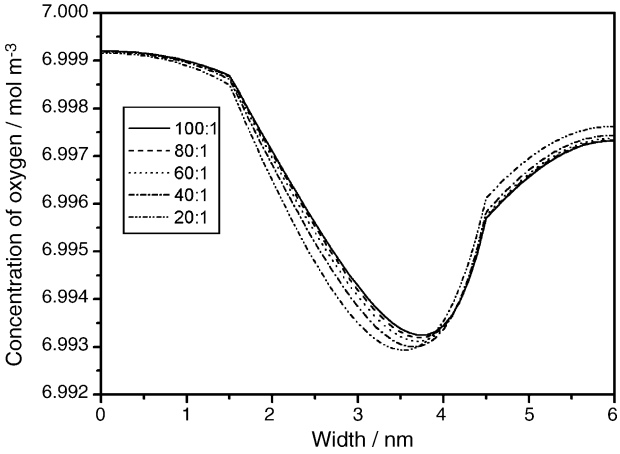

Fig. 15. Effect of the proportion of kp1 to kp2 on concentration of oxygen distribution at $x = 0.5L3$.

the quantity of the increasing becomes large near 20:1. It can be seen from Fig. 13 that the pressure difference between two neighbor channels increases as increasing kp1. But the velocity under the shoulders decreases with the rising of kp1 because the velocity in x-direction increases faster.

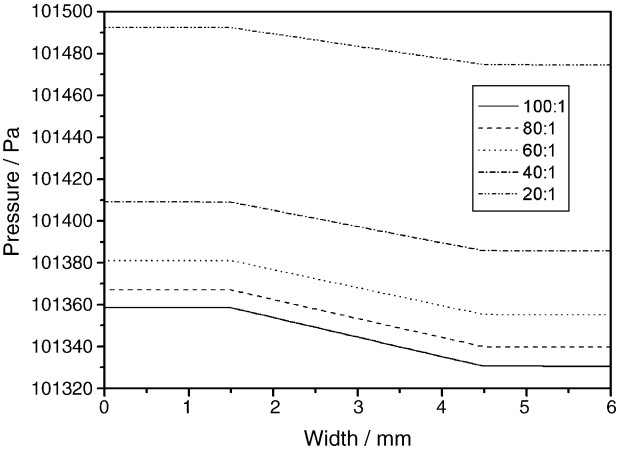

Fig. 13. Effect of the proportion of kp1 to kp2 on pressure distribution at $x = 0.5L3$.

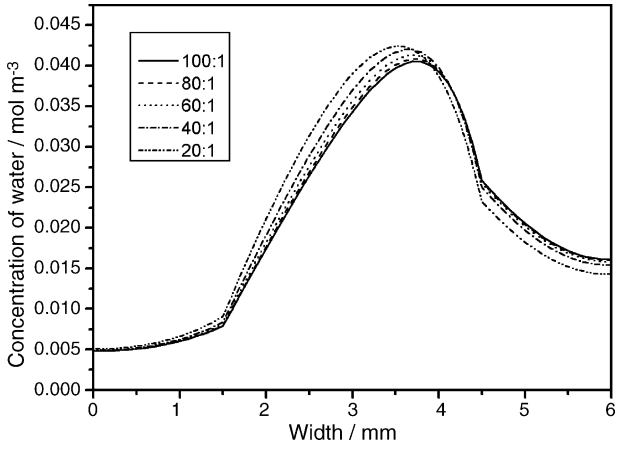

Fig. 16. Effect of the proportion of kp1 to kp2 on concentration of water distribution at $x = 0.5L3$.

The concentrations of oxygen and the water were shown in Figs. 15 and 16. However the distributions of oxygen and water also have relationship with the velocity at the ports. The velocity we selected here is different in neighbor channels and can help to distribute the oxygen in the NINO flow field. When the kp1 increases, the velocities decrease in channel and increase under shoulder. However the state of water is reverse, because of the constantly producing water.

The polarization curve under the five conditions was not given here, because the oxygen concentration in each condition is almost same to each other. It is mainly because the decreasing of oxygen concentration under shoulder counteracts the increasing of it in channel with the decreasing of kp1:kp2.

Therefore it is helpful to enhance the PEMFC performance in moving the water, as increasing the proportion of kp1 to kp2.

4.5. Effect of width of channel and shoulder

Effect of width of shoulder and channel was shown in Figs. 17–21. The width summation of the neighbor channel and shoulder was kept in constant value; the proportion of the channel and shoulder (W_{cha}:W_{sho}) was changed with the other parameters keeping as base case. The pressure distribution of the NINO flow field at $x = 0.5$L3 is shown in Fig. 17. When the width of channel decreases, the pressure increases in high-pressure channel, while decreases in low-pressure channel until W_{cha}:W_{sho} is 1:1 and then increases.

In addition, we can mention that the pressure difference varies with the changing of proportion. This causes the velocity under all shoulders shown in Fig. 18 increase until 1:2. However the velocity in channels increases all the time. Because of the variation of the velocity, the distributions of oxygen and water shown in Figs. 19 and 20 must redistribute. The concentration of oxygen increases only in high-pressure channel, but decreases in low-pressure channel and under shoulder. When the width of channel increases, the fluid in the NINO flow field becomes homogeneous. However, the homogeneous distribution of water has the reverse trends.

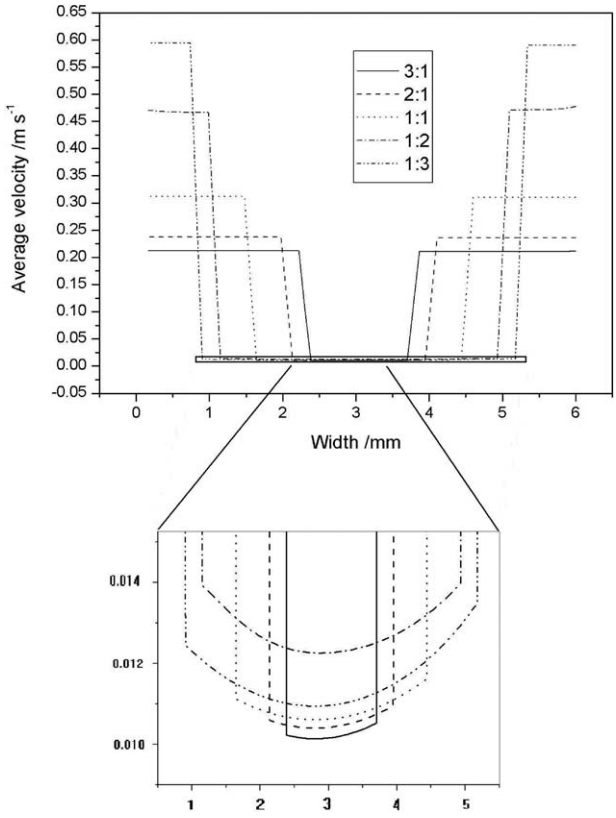

Fig. 18. Effect of width of shoulder and channel on the velocity distribution at $x = 0.5$L3.

The polarization curve was shown in Fig. 21. The continually increasing of the current has direct relation with the decreasing of width of channel. The intrinsic reason should be the high mass-transport activity under shoulder, though the concentration under shoulder decreases with the decreasing of W_{cha}:W_{sho}. This result is not like the result in the three-dimension model where there is an optimal proportion of width of channel to the width of shoulder [21]. It is mainly because of the assumption that the channel and GDL have the same height.

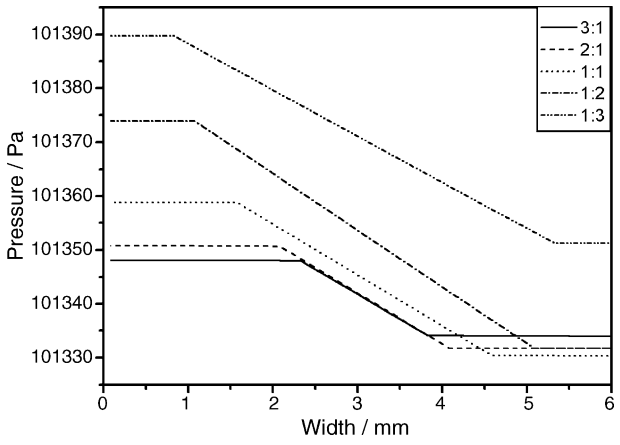

Fig. 17. Effect of width of shoulder and channel on the pressure distribution at $x = 0.5$L3.

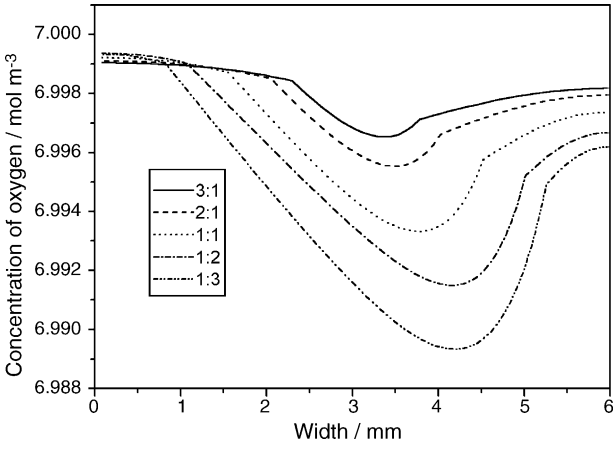

Fig. 19. Effect of width of shoulder and channel on the concentration of oxygen at $x = 0.5$L3.

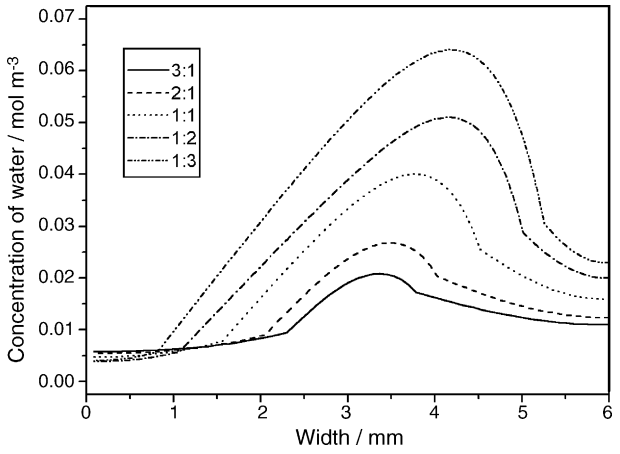

Fig. 20. Effect of width of shoulder and channel on the concentration of water at $x = 0.5L3$.

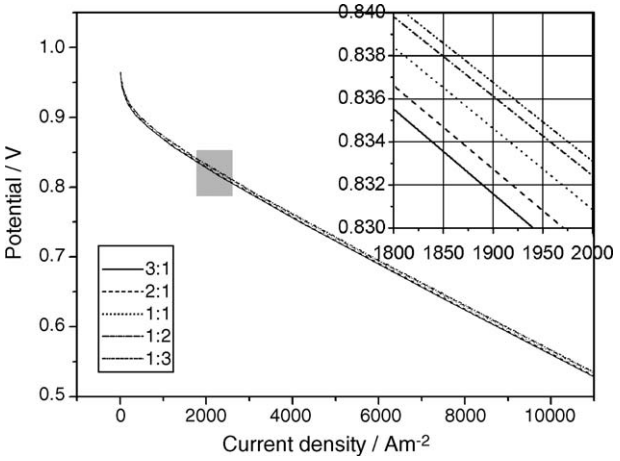

Fig. 21. Effect of width of shoulder and channel on polarization curve of a PEMFC.

5. Conclusions

The new flow field presented here can easily be transformed to the general one such as parallel and interdigitated flow field. There are $2n$ independent ports in the NINO. The ports in this paper are divided into four kinds: inlet1, inlet2, outlet1, outlet2 by different boundary condition at the ports. A two-dimension mathematic model was developed to describe the distribution of pressure, x-direction velocity, y-direction velocity, average velocity, oxygen, water and the polarization curve of the air cathode, which constructed by the NINO.

The numerically prediction shows good agreement with the newly selected experimental voltage versus current density at the different operating temperature.

With the increasing of k_p, the pressure decreases dramatically in high-pressure channel. But the other results such as x-direction velocity, y-direction velocity, average velocity, oxygen, water and the polarization curve will not change.

When the proportion of kp1 to kp2 increases, the velocities decrease in channel and increase under shoulder. As a result, the refreshment of oxygen increases fast in high-pressure channel and decreases under shoulder and in right channel, and the state of water is reverse. But it scarcely affects the polarization curve.

With the decreasing of W_{cha}:W_{sho}, the current continually increases because of the high mass-transport activity under shoulder, though the concentration under shoulder decreases.

Acknowledgments

The authors are grateful for the financial sponsors of State Key Fundamental Research Program of China (973 Program, G2000026408), State Key High Technology Research Program of China (863 Program, 2001AA323060, 2003AA517062), Nature Science Foundation of China (NSFC20373068).

References

[1] D. Natarajan, T.V. Nguyen, J. Power Sources 115 (2003) 66.
[2] M.G. Hu, A.Z. Gu, M.H. Wang, X.J. Zhu, Energy Convers. Manage. 45 (2004) 1861.
[3] U. Sukkee, C.Y. Wang, J. Power Sources 125 (2004) 40.
[4] J.S. Yi, T.V. Nguyen, J. Electrochem. Soc. 146 (1999) 38.
[5] A.A. Kornyshev, A.A. Kulikovsky, Electrochim. Acta 46 (2001) 4389.
[6] T.C. Jen, T.Z. Yan, S.H. Chan, Int. J. Heat Mass Transf. 46 (2003) 4157.
[7] S. Um, C.Y. Wang, K.S. Chen, J. Electrochem. Soc. 147 (2000) 4485.
[8] T. Berning, N. Djilali, J. Power Sources 124 (2003) 440.
[9] R. Hahna, S. Wagner, A. Schmitz, H. Reichl, J. Power Sources 131 (2004) 73.
[10] D.M. Bernardi, M.W. Verbrugge, J. Electrochem. Soc. 139 (1992) 2477.
[11] T.E. Springer, T.A. Zawodzinski, S. Gottesfeld, J. Electrochem. Soc. 138 (1991) 2334.
[12] T.F. Fuller, J. Newman, J. Electrochem. Soc. 140 (1993) 1218.
[13] V. Gurau, H. Liu, S. Kakac, AIChE J. 44 (1998) 2410.
[14] S. Um, C.Y. Wang, K.S. Chen, J. Electrochem. Soc. 145 (1998) 1149.
[15] A.C. West, J. Appl. Electrochem. 26 (1996) 557.
[16] H. Yang, T.S. Zhao, Q. Ye, J. Power Sources 139 (2005) 79.
[17] E.A. Ticianelli, C.R. Derouin, S. Srinivasan, J. Electroanal. Chem. 251 (1988) 275.
[18] T.E. Springer, T.A. Zawodzinski, S. Gottesfeld, J. Electrochem. Soc. 138 (1991) 2334.
[19] A. Parthasarathy, S. Srinivasan, J. Appleby, J. Electrochem. Soc. 139 (1992) 2530.
[20] M. Hu, X. Zhu, M. Wang, A. Gu, L. Yu, Energy Convers. Manage. 45 (2004) 1883.
[21] A. Kumar, R.G. Reddy, J. Power Sources 113 (2003) 11.
[22] R.C. Reid, J.M. Prausnitz, B.E. Poling, The Properties of Gases and Liquids, 4th, McGraw-Hill, New York, 1987.
[23] T.E. Springer, T.A. Zawodzinski, S. Gottesfeld, J. Electrochem. Soc. 140 (1993) 3513.
[24] V.N. Trung, W. Ralphe, J. Electrochem. Soc. 140 (1993) 2178.